Hindawi
Geofluids
Volume 2018, Article ID 4023150, 15 pages
https://doi.org/10.1155/2018/4023150

Research Article

Fractal Analysis of Microscale and Nanoscale Pore Structures in Carbonates Using High-Pressure Mercury Intrusion

Fuyong Wang[1], **Peiqing Lian**[2], **Liang Jiao**[1], **Zhichao Liu**[1], **Jiuyu Zhao**[1] and **Jian Gao**[3]

[1]*Research Institute of Enhanced Oil Recovery, China University of Petroleum (Beijing), Beijing 102249, China*
[2]*Petroleum Exploration and Development Research Institute, SINOPEC, Beijing 100083, China*
[3]*State Key Laboratory of Enhanced Oil Recovery, Research Institute of Petroleum Exploration and Development, Beijing 100083, China*

Correspondence should be addressed to Fuyong Wang; wangfuyong@cup.edu.cn

Received 8 September 2017; Accepted 17 January 2018; Published 7 June 2018

Academic Editor: Timothy S. Collett

This paper investigated fractal characteristics of microscale and nanoscale pore structures in carbonates using High-Pressure Mercury Intrusion (HPMI). Firstly, four different fractal models, i.e., 2D capillary tube model, 3D capillary tube model, geometry model, and thermodynamic model, were used to calculate fractal dimensions of carbonate core samples from HPMI curves. Afterwards, the relationships between the calculated fractal dimensions and carbonate petrophysical properties were analysed. Finally, fractal permeability model was used to predict carbonate permeability and then compared with Winland permeability model. The research results demonstrate that the calculated fractal dimensions strongly depend on the fractal models used. Compared with the other three fractal models, 3D capillary tube model can effectively reflect the fractal characteristics of carbonate microscale and nanoscale pores. Fractal dimensions of microscale pores positively correlate with fractal dimensions of the entire carbonate pores, yet negatively correlate with fractal dimensions of nanoscale pores. Although nanoscale pores widely develop in carbonates, microscale pores have greater impact on the fractal characteristics of the entire pores. Fractal permeability model is applicable in predicting carbonate permeability, and compared with the Winland permeability model, its calculation errors are acceptable.

1. Introduction

Compared with sandstones, carbonate pore structures are usually more complex. There are many diverse types of pore space in carbonates such as intergranular pores, intraparticle pores, moldic pores, fractures, and vugs. Generally, carbonate reservoirs are more heterogeneous and flow mechanisms are more intricate, making carbonate reservoir development problematic. The Y oil reservoir is a porous carbonate reservoir in the Middle East[1, 2]. Even though fractures and vugs develop in carbonates, grain pores are the main oil storage space. In this paper, HPMI technique was utilized to describe the sizes and distributions of carbonate microscale and nanoscale pores, and the fractal characteristics of microscale and nanoscale pores were also investigated.

Since Mandelbrot first proposed the fractal theory in 1980s [3], its application has been widely used for rock pore structure characterization, due to its effectiveness in describing complex and irregular structures with self-similar characteristics. The microstructures of rock pore space have been proven to be fractal [4–6]. With scanning electron microscopy (SEM), Katz and Thompson [7] demonstrated that sandstone pore space is fractal and self-similar with over 3 to 4 orders of magnitude. Angulo et al. [8] calculated fractal dimensions of sandstone using mercury intrusion test. Ever since, mercury intrusion method has been extensively used to study fractal characteristics of pore structures in sandstones [9–11] and coals [12–14]. On the other hand, nitrogen adsorption technique is widely used to analyse the fractal characteristics of nanoscale pores in shales [15–17]. The fractal characteristics of carbonate pores have been expansively studied by many scholars. Krohn [18] studied fractal characteristics of carbonate pores with SEM. Xie [19] calculated fractal dimensions of carbonate pores using

box-counting method from environmental scanning electron microscope (ESEM) images and indicated that carbonate pores are multifractal. The previous studies have demonstrated that fractal dimension can effectively reflect roughness of pore surface and characterize heterogeneity of pore structures.

Accurately predicting carbonate permeability is challenging due to high heterogeneity in carbonate pore structures. Several models proposed have been commonly used to estimate carbonate permeability, including Purcell model [20], Winland model [21], Swanson model [22], and Pittman model [22]. Besides pore structure analysis, fractal theory has also been used to predict porous media permeability [23, 24]. One of the most broadly used methods was proposed by Yu and Cheng [23]; their model was developed based on the tortuous fractal capillary tube model, although no empirical parameters were introduced in their model. Similarly, based on the tortuous and fractal tubular bundle model, Buiting and Clerke [25] developed a different fractal permeability model, which had been verified with more than 500 carbonate core samples, but empirical parameters were introduced. With more than 200 carbonate core samples, Nooruddin et al. [26] compared nine different permeability models using mercury intrusion capillary pressure data, and they found that Swanson and Winland permeability models gave the best carbonate permeability prediction results. However, Yu and Cheng's permeability model was not evaluated in their studies. In this paper, the adaptability of Yu and Cheng's permeability model for carbonate permeability prediction was evaluated and compared with Winland model.

2. HPMI

16 core samples collected from the Y carbonate reservoir were used for this study. The pore space of these carbonate core samples excludes visible fractures and vugs. The measured air permeability and porosity of core samples are shown in Table 1. The porosity of core samples varies from 12.485% to 31.805%, with an average of 17.526%, and air permeability varies from 0.591 mD to 70.556 mD with an average of 12.380 mD. As shown in Figure 1, porosity-permeability correlation is very weak, indicating high heterogeneity of carbonate core samples.

Pore structures and pore size distributions of carbonate core samples were characterized with HPMI technique. In the experiment, the Auto Pore III-9420 was used, and the maximum mercury intrusion capillary pressure is approximately 276 MPa. Figure 2 presents mercury intrusion capillary pressure curves of all the core samples. Mercury is nonwetting to rock surface and has a high surface tension with air. With mercury intrusion pressure increasing, nonwetting mercury enters the small pores of the core samples, and the pore radius can be calculated from the Washburn equation [28]:

$$P_c = \frac{2\sigma \cos\theta}{r} \quad (1)$$

where P_c is the mercury intrusion capillary pressure; r is pore radius; σ is the interfacial tension between mercury and air; and θ is mercury and rock contact angle. Under the maximum intrusion pressure, the corresponding minimum pore radius that can be detected is 2.7 nm. The structures and distributions of almost the entire pores, from nanoscale pores to microscale pores, were tested during the HPMI test, and then the parameters of pore structure were calculated from HPMI curves as shown in Table 2.

Table 1: Air permeability and porosity of carbonate core samples.

Core No.	Porosity ϕ (%)	Air permeability K_{air} (mD)
1	31.805	70.556
2	13.752	1.220
3	18.537	1.515
4	14.579	1.164
5	19.676	1.696
6	16.481	0.591
7	18.541	1.002
8	19.145	1.814
9	15.174	1.106
10	20.059	1.103
11	22.190	18.392
12	13.787	12.844
13	14.083	24.300
14	16.089	38.170
15	14.040	13.832
16	12.485	8.772

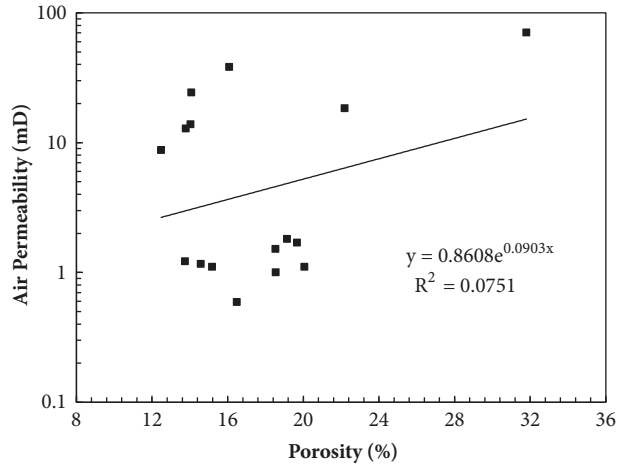

Figure 1: Porosity-permeability correlation of 16 carbonate core samples.

3. Methodology Description

According to fractal geometry theory, when pore structures are fractal, the relationship between the pore number and pore radius can be presented as [3]

$$N(>r) \propto r^{-D_f} \quad (2)$$

Table 2: Pore structure parameters of carbonate core samples obtained from HPMI test.

Core No.	Displacement pressure P_d (MPa)	Maximum pore radius r_{max} (μm)	r_{50} (μm)	r_{35} (μm)	Sorting coefficient S_p	Skewness S_{kp}	Tortuosity τ
1	0.139	5.738	1.021	1.471	2.643	0.414	1.443
2	0.244	3.672	0.813	1.037	2.108	0.341	6.812
3	0.869	0.965	0.366	0.413	1.682	0.169	10.229
4	0.692	1.258	0.441	0.462	1.119	0.320	5.212
5	1.033	0.791	0.456	0.444	1.839	-0.029	11.880
6	0.689	1.251	0.517	0.539	1.068	0.386	5.680
7	1.033	0.790	0.345	0.339	0.846	0.340	6.307
8	1.202	0.668	0.328	0.341	2.377	-0.045	11.407
9	0.863	0.967	0.238	0.277	1.926	-0.149	10.381
10	1.202	0.667	0.327	0.324	1.081	0.449	9.658
11	0.243	3.679	1.245	1.412	1.798	0.495	2.219
12	0.251	3.629	0.850	1.293	3.005	0.035	3.774
13	0.243	3.679	1.094	1.582	2.338	0.334	2.235
14	0.156	5.065	0.686	1.364	2.660	0.190	1.638
15	0.156	5.065	0.907	1.576	2.998	0.092	3.242
16	0.087	9.588	2.295	2.903	3.431	0.298	4.394

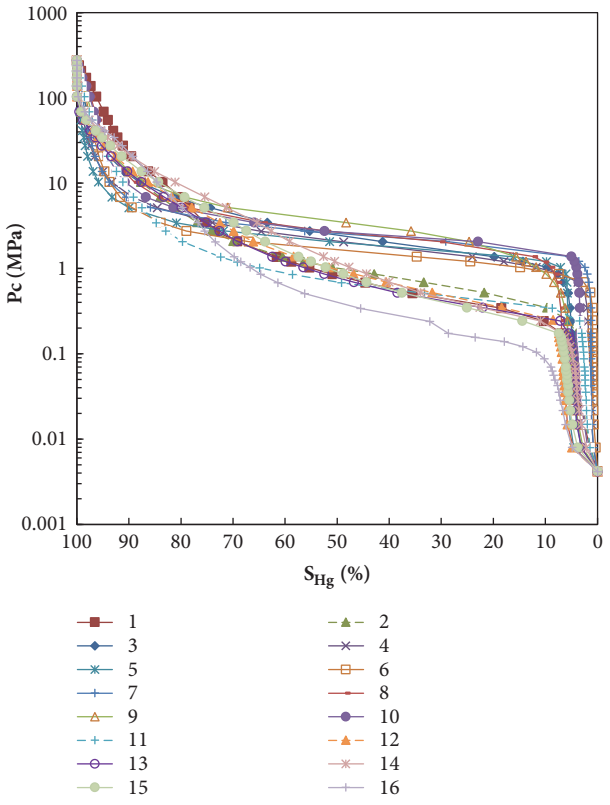

Figure 2: Mercury intrusion capillary pressure curves of 16 carbonate core samples.

where r is the pore radius (characteristic length); $N(>r)$ is pore number with pore radius larger than r; and D_f is fractal dimension. There are several different methods to calculate pore number $N(>r)$ based on different assumptions. In this paper, four different fractal models were used to calculate fractal dimensions from mercury intrusion capillary pressure curves, and the most suitable fractal model was selected to analyse the fractal characteristics of microscale and nanoscale pore structures.

3.1. I-2D Capillary Tube Model Method. In this method, pore networks of core samples are made up of a bundle of tortuous capillary tubes. The numbers of capillary tubes with tube radius r can be calculated with the volume of mercury intrusion as given by

$$n(r) = \frac{\triangle V_{Hg}(r)}{\pi r^2 l} \tag{3}$$

where $n(r)$ is the number of capillary tubes with radius r; $\triangle V_{Hg}(r)$ is the single volume of mercury intrusion at radius r; and l is the core length. Then the cumulative number $N(>r)$ can be calculated as

$$N(>r) = \int_r^{r_{max}} n(r)\, dr. \tag{4}$$

According to (2), fractal dimension D_f can be determined from the slope of the line of $\lg N(>r)$ and $\lg r$ in a log-log plot.

3.2. II-3D Capillary Tube Model Method. Instead of using single volume of mercury intrusion $\triangle V_{Hg}(r)$, Li [9] used the cumulative volume of mercury intrusion V_{Hg} to

calculate the number of filled capillary tubes $N(r)$ as given by

$$N(r) = \frac{V_{Hg}}{\pi r^2 l}. \quad (5)$$

Substituting (5) into (2),

$$\frac{V_{Hg}}{\pi r^2 l} \propto r^{-D_f}. \quad (6)$$

The core length l is constant, and therefore (6) can be simplified as

$$V_{Hg} \propto r^{2-D_f}. \quad (7)$$

As V_{Hg} can be expressed with mercury saturation S_{Hg}, and pore radius r can be expressed with mercury intrusion capillary pressure P_c, (7) can be expressed as

$$S_{Hg} \propto {p_c}^{-(2-D_f)}. \quad (8)$$

Then fractal dimension D_f can be calculated from the $\lg S_{Hg}$–$\lg p_c$ plot. With the same datapoints, the calculated fractal dimensions using (6) and (8) should be the same.

Although methods I and II are based on the capillary tube model, they are essentially different. Method I reflects the fractal characteristics of the capillary tube distribution in the cross-section of core samples, which is in two-dimensional space, and the range of the calculated fractal dimension using method I is $1 < D_f < 2$. Method II obtains fractal dimension by filling pore space of core samples with different size of capillary tubes, which can reflect the fractal characteristics of pore space in three-dimensional space, and generally the calculated fractal dimension using method II is $2 < D_f < 3$.

3.3. III-Geometry Model Method. Based on the geometry fractal characteristics of coals, Friesen and Mikula [29] proposed an equation to calculate fractal dimension which can be expressed as

$$\frac{dS_{Hg}}{dp_c} \propto {p_c}^{-(4-D_f)}. \quad (9)$$

The fractal dimension D_f was calculated by plotting dS_{Hg}/dp_c verse p_c in a log-log plot.

3.4. IV-Thermodynamic Model Method. Based on the thermodynamic analysis of mercury intrusion process and fractal characteristics of pore surface, Zhang and Li [30] proposed a thermodynamic model, and the simplified equation for calculating fractal dimension can be expressed as [31]

$$\ln\left(\frac{W_n}{r_n^2}\right) = D_f \ln\left(\frac{V_n^{1/3}}{r_n}\right) + C \quad (10)$$

where W_n is the cumulative surface energy during the mercury intrusion process; r_n is pore radius; and V_n is the intrusion volume of mercury at stage n.

The calculated fractal dimensions using method III and IV reflect the volume heterogeneity and surface heterogeneity of carbonate pores, respectively [12, 32].

Table 3: The fractal dimensions of entire pores using different fractal models.

Core No.	Fractal dimensions			
	Method I D_{f1}	Method II D_{f2}	Method III D_{f3}	Method IV D_{f4}
1	1.853	2.296	2.777	2.679
2	1.640	2.253	2.428	2.574
3	1.585	2.335	2.433	2.549
4	1.441	2.367	2.274	2.451
5	1.267	2.298	2.059	2.427
6	1.480	2.338	2.356	2.430
7	1.518	2.448	2.325	2.467
8	1.559	2.281	2.413	2.537
9	1.674	2.355	2.504	2.594
10	1.614	2.367	2.503	2.547
11	1.602	2.231	2.523	2.537
12	1.562	2.213	2.678	2.592
13	1.509	2.199	2.624	2.557
14	1.772	2.276	2.858	2.683
15	1.733	2.256	2.858	2.680
16	1.774	2.215	2.763	2.689
Average	1.599	2.295	2.532	2.562

4. Fractal Dimension Calculation

The calculated fractal dimensions using methods I, II, III, and IV were expressed as D_{f1} D_{f2}, D_{f3}, and D_{f4}, respectively. The no. 2 core sample was selected as an example to demonstrate the process of fractal dimension calculation using four methods presented above. As depicted in Figure 3, fractal dimensions were calculated from the slope of straight line in log-log plots. All carbonate pores, from the maximum pore radius to the minimum pore radius, were selected for linear fitting, and therefore the calculated fractal dimensions reflect the average fractal characteristics of entire carbonate pores, including microscale pores and nanoscale pores. Method I, method III, and method IV have good linear fitting results, and the determination coefficients are larger than 0.96. However, for method II, the determination coefficient of the linear fitting is less than 0.60, the curve of $\lg S_{Hg} - \lg p_c$ breaks into two segments, and the linear fitting result with one straight line is poor.

Table 3 shows the calculated fractal dimensions with the four methods. The results show that the calculated fractal dimensions depend on the methods used. The calculated fractal dimensions with method I D_{f1} vary from 1.267 to 1.853, indicating that D_{f1} reflects fractal characteristics of pore distribution in two-dimensional space. The calculated fractal dimensions with methods II, III, and IV are between 2 and 3, which means D_{f2}, D_{f3}, and D_{f4} reflect fractal characteristics of pore structures in three-dimensional space. Overall, D_{f3} and D_{f4} are close to each other, but larger than D_{f2}.

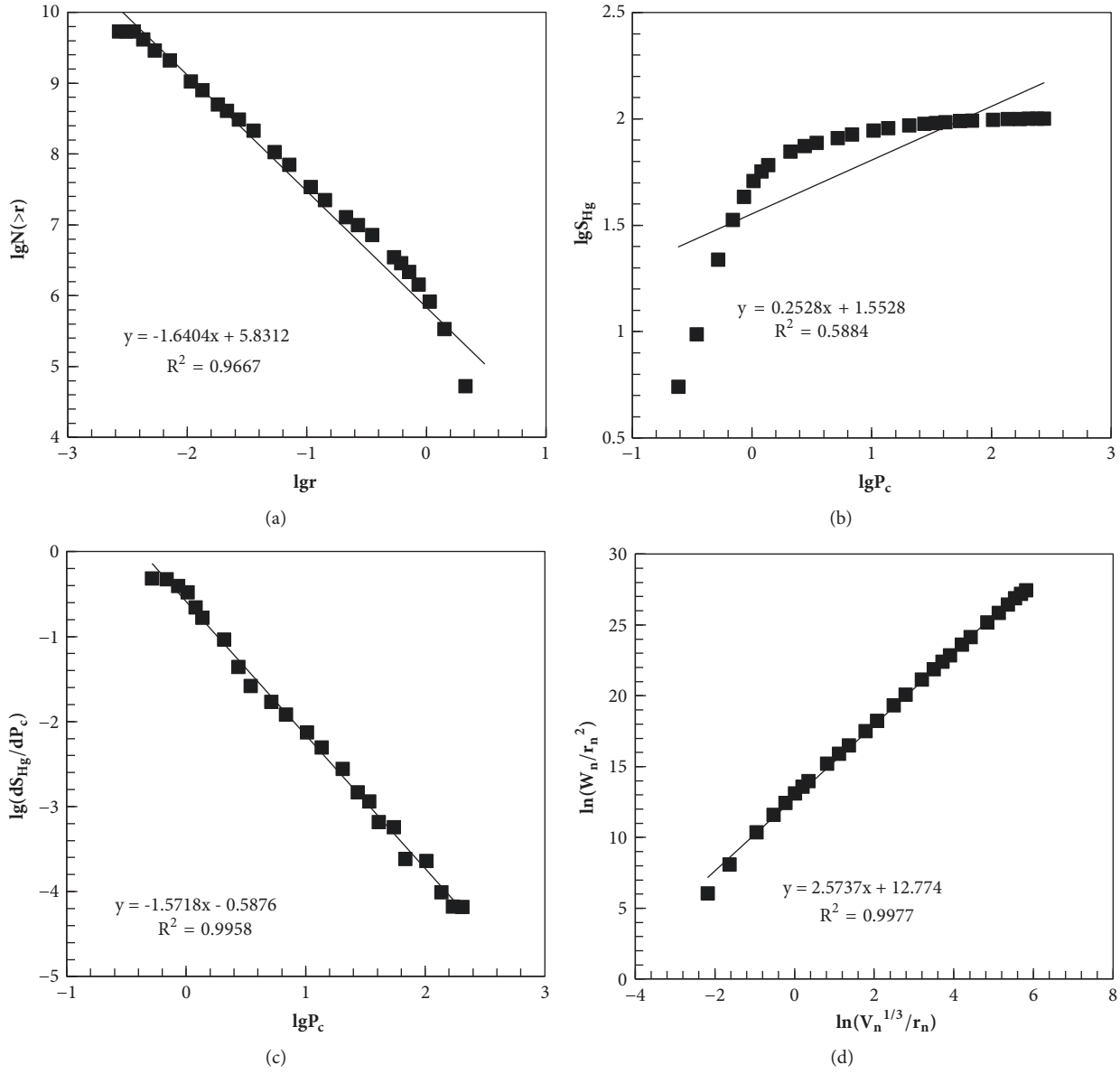

Figure 3: Fractal dimension calculation from the slope of straight line in log-log plots with different methods ((a) method I-2D capillary tube model; (b) method II-3D capillary tube model; (c) method III-geometry model; (d) method IV-thermodynamics model).

To study the fractal characteristics of microscale pores and nanoscale pores, respectively, method II was used to calculate the fractal dimensions of microscale pores and nanoscale pores by fitting the curve of $\lg S_{Hg} - \lg p_c$ with two straight lines. As shown in Figure 4, the determination coefficients of linear fitting with two straight lines are much larger than that of linear fitting with one straight line, which indicates that microscale pores and nanoscale pores have different fractal characteristics.

Table 4 presents the calculated fractal dimensions of microscale pores $D_{f2\mathrm{m}}$ and nanoscale pores $D_{f2\mathrm{n}}$. The fractal dimensions of microscale pores $D_{f2\mathrm{m}}$ vary from 3.006 to 5.044 and are much larger than the fractal dimensions of nanoscale pores $D_{f2\mathrm{n}}$, which vary from 2.028 to 2.122, indicating that pore structures of microscale pores are complex than those of nanoscale pores. According to fractal theory, the calculated fractal dimension in three-dimensional space should be less than 3. The reason for $D_{f2\mathrm{m}}$ being greater than 3 may be the oversimplification of cylinder shape of microscale pores [10]. When (8) was derived from (7), the assumption was that that the shape of the pores is cylindrical, hence rendering (1) valid. However, for the microscale pores, especially for the carbonates, fractures and large pores with complex shapes may exist, which can lead to the value of $D_{f2\mathrm{m}}$ beyond 3.

Figure 5 shows the relationship between the fractal dimensions of the entire microscale and nanoscale pores. The fractal dimensions of microscale pores $D_{f2\mathrm{m}}$ strongly agree with the fractal dimensions of the entire pores D_{f2}, but poorly correlate with the fractal dimensions of nanoscale

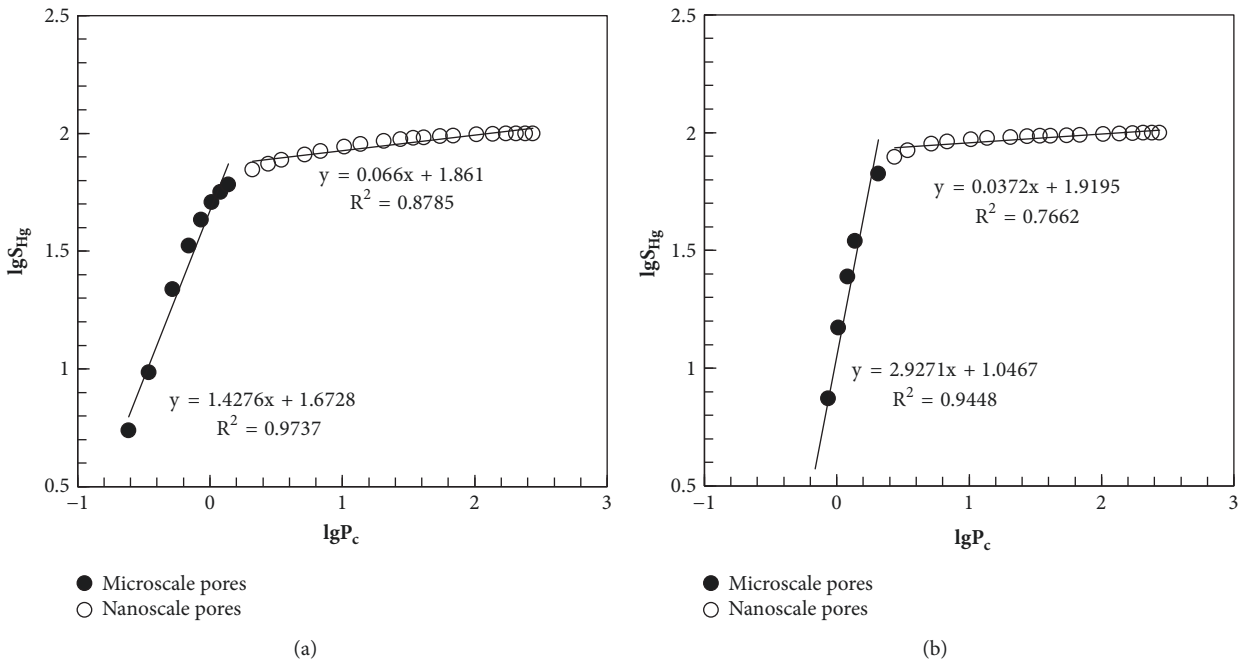

Figure 4: Fractal dimensions calculation for nano- and micropores with method II using two-straight-line fitting ((a) no. 2 core sample; (b) no. 6 core sample).

Table 4: The fractal dimensions of microscale pores and nanoscale pores calculated with method II using two-straight-line fitting.

Core sample No.	Microscale pores		Nanoscale pores	
	Pore size range (μm)	Fractal dimension D_{fm}	Pore size range (μm)	Fractal dimension D_{fn}
1	0.7279-5.3582	3.259	0.0027-0.6226	2.084
2	0.5412-3.0502	3.428	0.0027-0.3549	2.066
3	0.2145-0.8553	3.616	0.0027-0.1443	2.057
4	0.2716-1.0746	4.078	0.0027-0.2152	2.046
5	0.2693-0.7197	4.482	0.0027-0.2163	2.031
6	0.3598-1.0786	4.927	0.0027-0.2706	2.037
7	0.2159-0.7192	5.044	0.0027-0.1434	2.028
8	0.2153-0.6184	3.845	0.0027-0.1431	2.047
9	0.1429-0.8607	3.131	0.0027-0.1077	2.047
10	0.2156-0.6181	4.824	0.0027-0.1432	2.039
11	0.7289-3.0633	4.117	0.0027-0.6229	2.055
12	0.5388-2.9625	3.061	0.0027-0.3609	2.079
13	0.8634-3.0627	3.512	0.0027-0.7205	2.094
14	0.7162-4.7693	3.126	0.0027-0.6114	2.122
15	0.8642-4.7698	3.200	0.0027-0.7211	2.111
16	1.4593-8.5343	3.006	0.0027-1.0897	2.079

pores D_{f2n}, and with D_{f2m} increasing, D_{f2n} decreases. It can be concluded that fractal characteristics of nanoscale pores and microscales pores are different, and microscale pores have greater impact on the fractal characteristics of the entire pores compared with nanoscale pores.

Lai et al. [10] also used $\lg S_{Hg} - \lg p_c$ plot to study the fractal characteristics of pore structures in tight gas sandstones. They found that nanoscale pores of tight sandstone can represent the fractal characteristics of entire pores much better than the microscale pores, which is opposite to the

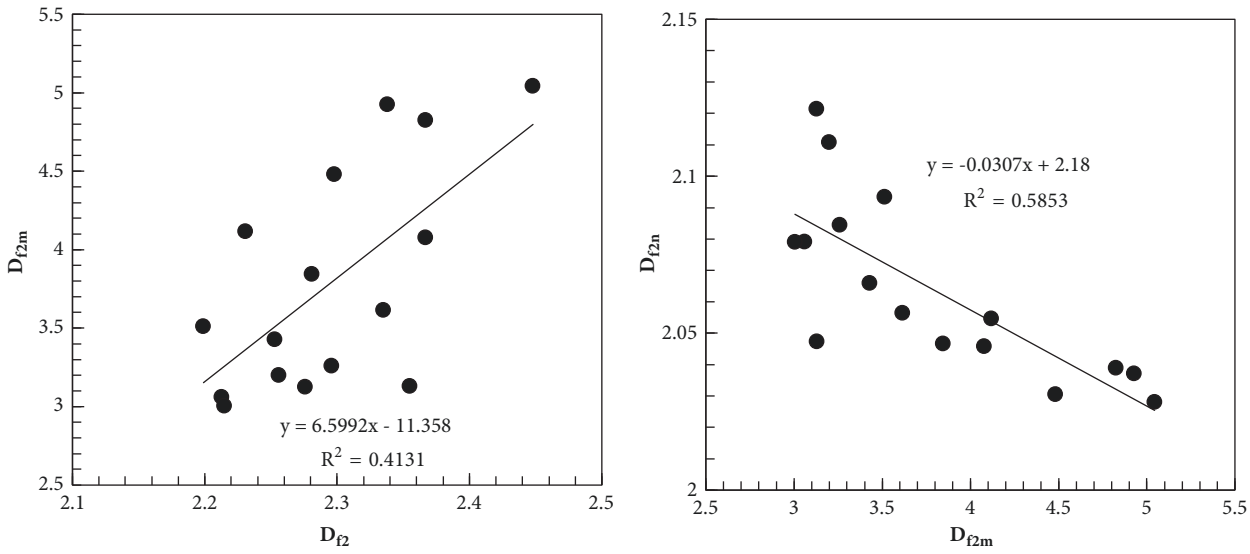

FIGURE 5: The relationship between fractal dimensions of entire pores D_{f2}, microscale pores D_{f2m}, and nanoscale pores D_{f2n} ((a) the relationship between fractal dimensions of the entire pores D_{f2} and fractal dimensions of microscale pores D_{f2m}; (b) the relationship between fractal dimensions of microscale pores D_{f2m} and fractal dimensions of nanoscale pores D_{f2n}).

results derived from carbonates studied in this paper. The different deductions may be caused by the difference in pore networks between carbonates and tight sandstones. The porosity of the carbonate core samples studied in this paper is much higher than that of tight sandstones. The nanoscale pores of these carbonates are not well connected, and carbonate pore networks are dominated by microscale pores, such as nonvisible microfractures, which have better connectivity.

5. Fractal Characteristic Analysis

The fractal dimensions calculated with the four methods are not the same. The relationships between the carbonate petrophysical properties and the fractal dimensions calculated with the four different methods, D_{f1}, D_{f2}, D_{f3}, and D_{f4}, were evaluated. Figure 6 shows the correlations between the air permeability K_{air} of core samples and the fractal dimensions calculated from the four different methods. In contrast, with D_{f2} increasing, K_{air} decreases logarithmically; however, D_{f1}, D_{f3}, and D_{f4} strongly agree with K_{air}. According to Liu et al. [33], for the fractal capillary tube model, the poor correlation between permeability and fractal dimension is reasonable, which means D_{f2} is more suitable for fractal analysis of carbonate pore structures and petrophysical properties. As depicted in Figure 7, with D_{f2} increasing, displacement pressure P_d and tortuosity τ increase and pore radius r_{50} and r_{35} decrease, indicating pore structures become more complex.

Hydraulic Flow Unit (HFU) identification is imperative in reservoir characterization. Amaefule et al. [33] first introduced the reservoir quality index/flow zone indicator (RQI/FZI) method to identify HFU. Figure 8 shows the relationship between fractal dimensions of the entire pores D_{f2} and RQI and FZI. The results after the investigation showed that reservoir quality becomes poorer when RQI and FZI decrease with increasing D_{f2}. Using the improved HFU identification method proposed by Mirzaei-Paiaman et al. [27], HFUs were identified with the carbonate core samples studied in this paper. As indicated in Figure 9, the 16 carbonate core samples belong to two different HFUs, i.e., HFU-1 and HFU-2. The average fractal dimensions of HFU-1 and HFU-2 were calculated and are 2.34 and 2.24 respectively. The higher the quality of the HFU is, the lower the average fractal dimension will be.

The fractal characteristics of the microscale pores and nanoscale pores were analysed. Figures 10 and 11 present the fractal analysis of carbonate petrophysical properties using D_{f2m} and D_{f2n}, respectively. Comparatively, fractal analysis using D_{f2} in Figure 7 and D_{f2m} provided similar results, unlike D_{f2n} which gave different result, and it can be inferred that fractal dimensions of nanoscale pores D_{f2n} cannot be used for fractal analysis.

The distributions of pore volume and permeability contribution for microscale pores and nanoscale pores were calculated. Figure 12 presents the result of the no. 2 core sample. The pore radius distribution was from several nanometers to dozens of micrometers with bimodal distribution. The first and second peaks appeared around 0.1 μm and 1 μm, respectively. Although nanoscale pores were widely predominant, microscale pores contributed to most of the permeability. The distribution of permeability contribution is unimodal, and the peak appears at the same location of the maximum volume of microscale pores.

Table 5 illustrates the total pore volume and permeability contribution of microscale pores and nanoscale pores.

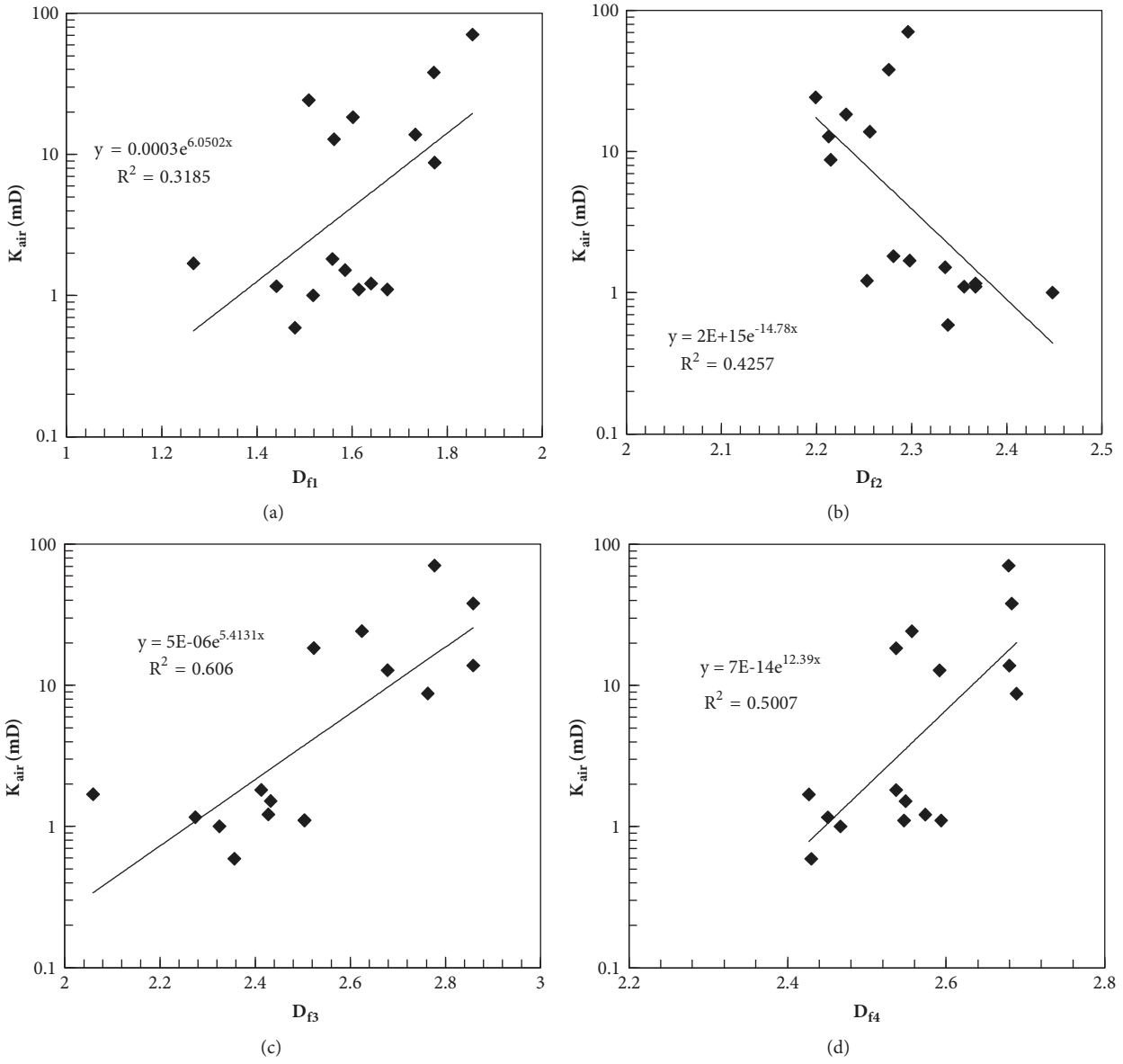

Figure 6: The correlation between the air permeability K_{air} and the fractal dimensions calculated from different methods.

Although nanoscale pores averagely occupy more than 38% of total pore volume, the average permeability contribution is less than 4%. Even for the no. 2 core sample, nanoscale pores only contributed 0.79% of the total permeability. Contrarily, microscale pores averagely contribute more than 96% of the total permeability, though the average volumes of microscale pores are only 55.14%. It could be concluded that though nanoscale pores are predominant in the Y carbonate reservoir, petrophysical properties are mainly dominated by microscale pores. Figure 13 presents the relationship between the permeability contributions and fractal dimensions of microscale and nanoscale pores. As shown in the figure, the permeability contribution of microscale pores and nanoscale pores decreases with increasing fractal dimensions. It can be explained that the increasing fractal dimensions indicated much complexity in the pore structures, which can in turn result in reduced permeability contribution.

6. Carbonate Permeability Modelling

Winland permeability model is an empirical equation considering the effect of pore size distribution on permeability, and it has been commonly used for predicting carbonate permeability. The Winland permeability model is expressed as [21]

$$\log r_{35} = 0.732 + 0.588 \log K - 0.864 \log \phi \quad (11)$$

where r_{35} is the pore radius with 35% mercury saturation and ϕ is porosity. Figure 14 presents the calculated permeability

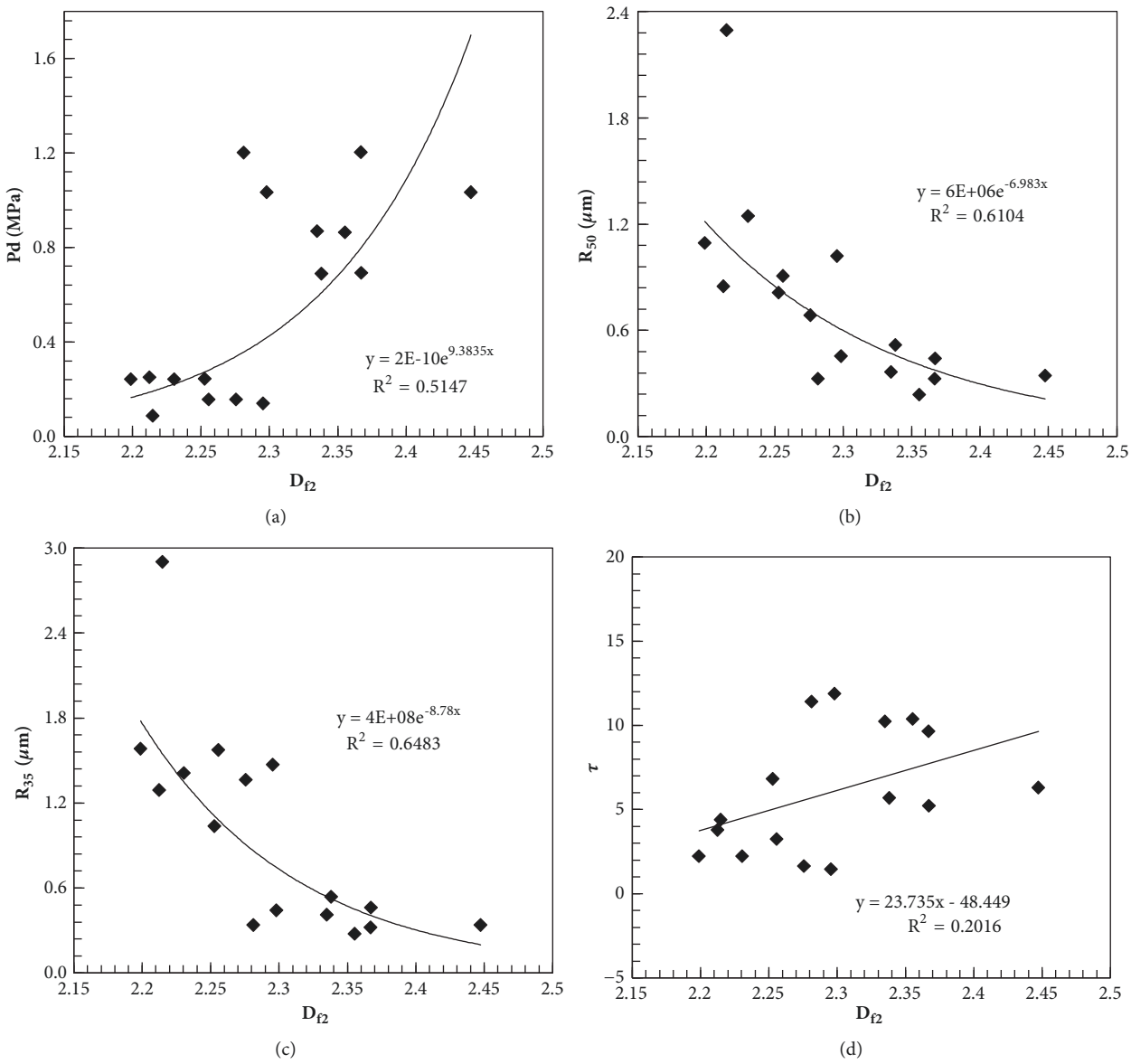

FIGURE 7: Relationship between fractal dimensions of the entire pores D_{f2} and some pore structure parameters and petrophysical properties of carbonate core samples ((a) D_{f2} and displacement pressure p_d; (b) D_{f2} and r_{50}; (c) D_{f2} and r_{35}; (d) D_{f2} and tortuosity τ).

using Winland permeability model compared with the measured air permeability. Overall, the calculated permeability is smaller than the measured air permeability. It may be due to the natural microfractures existing in carbonate core samples, which can enhance the permeability of the core samples.

The fractal permeability model proposed by Yu and Cheng is based on the tortuous fractal capillary tube model which can be expressed as [23]

$$K = \frac{\pi}{128}\frac{L_0^{1-D_T}}{A}\frac{D_f}{3+D_T-D_f}\lambda_{\max}^{3+D_T} \quad (12)$$

where L_0 is the representative length; A is the total section area and $A = L_0^2$; D_T is the tortuosity fractal dimension, and it can be calculated with the average tortuosity which can be measured from HPMI; and $\lambda_{\max}$ is the maximum pore diameter. As (12) is based on the tortuous capillary tube model, the two-dimensional fractal dimension should be used. Therefore, the fractal dimensions calculated with method I D_{f1} were used to predict carbonate permeability. Figure 15 shows the comparison between the calculated permeability using (12) and the measured permeability. Considering how heterogeneous carbonate pore structures are, the calculation errors are acceptable. The calculation errors may be due to the different fractal characteristics of microscale pores and nanoscale pores. In general, the fractal permeability model can be applied to model the permeability of porous carbonates without visible fractures and vugs.

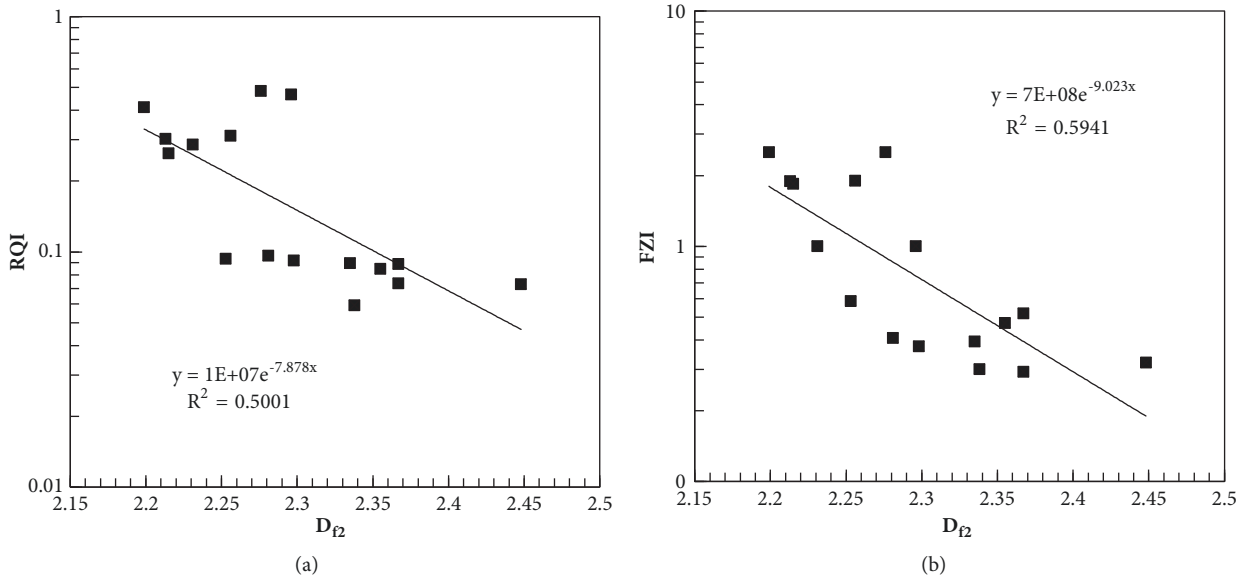

Figure 8: Relationship between fractal dimensions of the entire pores D_{f2} and RQI (a) and FZI (b).

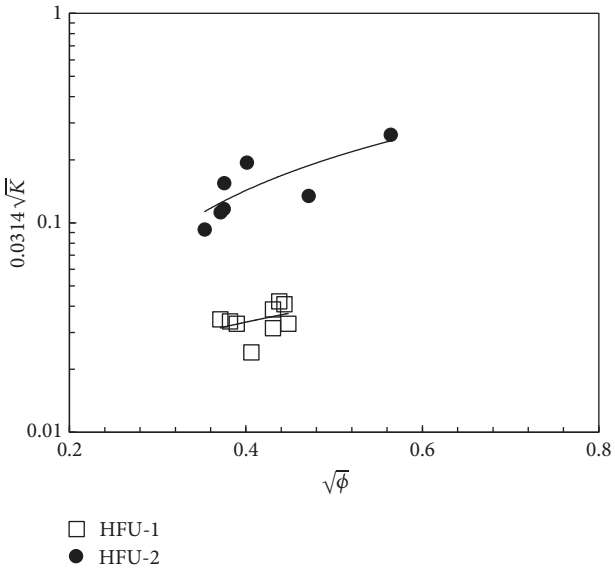

Figure 9: HFU identification with the improved method proposed by Mirzaei-Paiaman et al.[27].

7. Conclusion

Fractal theory was used to analyse microscale and nanoscale pore structures and petrophysical properties of carbonates with HPMI. The following conclusions can be drawn from this study:

(i) The calculated fractal dimensions strongly depend on the fractal models used. When carbonate pore space is assumed to be made up of bundles of capillary tubes, 3D capillary tube model can effectively analyse fractal characteristics of carbonate pore structures. Strong and correct correlations between carbonate petrophysical properties and fractal dimension calculated from 3D capillary tube model have been observed.

(ii) Microscale pores instead of nanoscale pores can represent the fractal characteristics of the entire pores of the carbonates in the Y oil reservoir. With the fractal dimensions increasing, the permeability contribution of microscale pores and nanoscale pores can both be reduced.

(iii) Fractal permeability model proposed by Yu and Cheng is applicable in predicting the permeability of

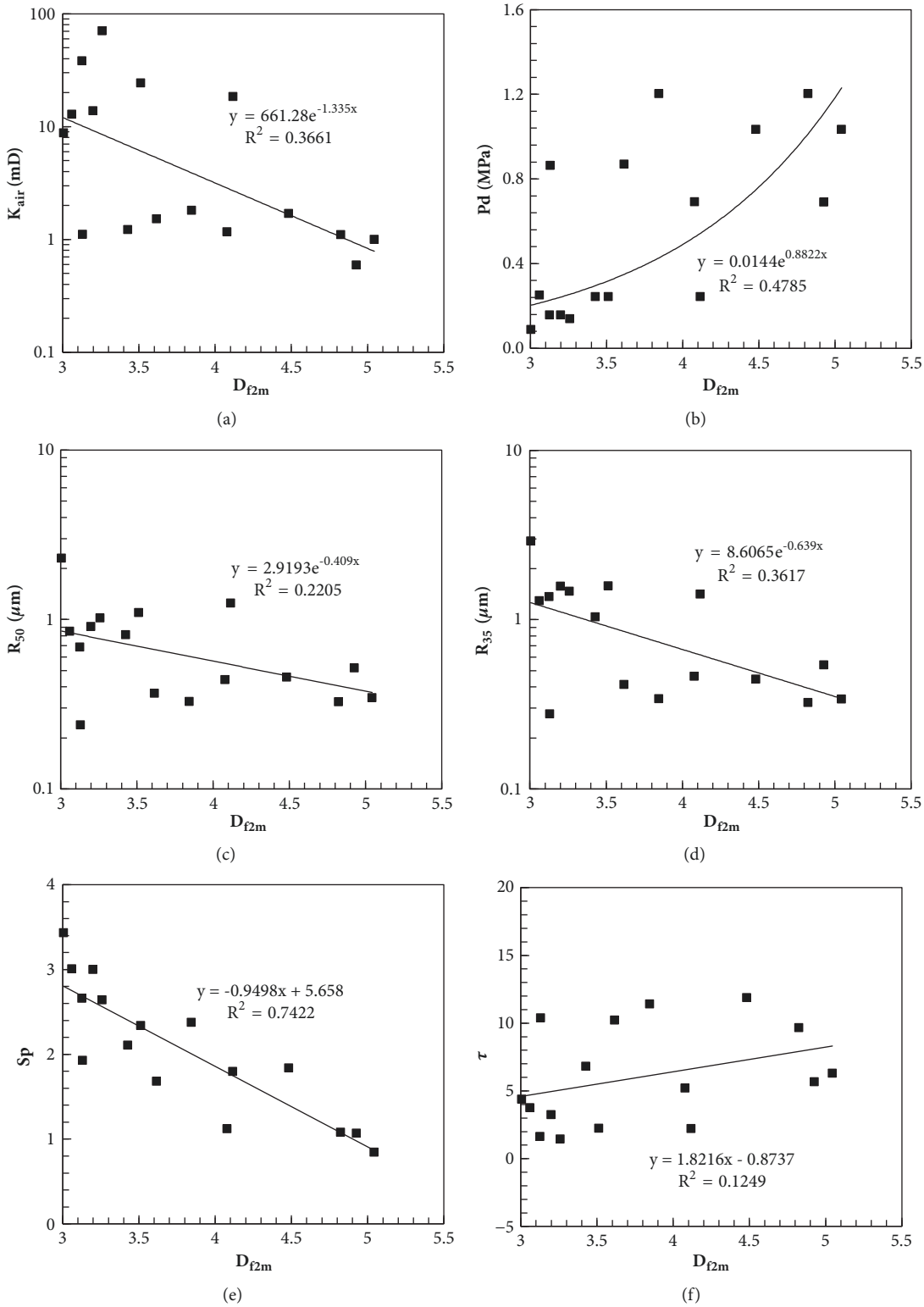

Figure 10: Relationship between fractal dimensions of microscale pores D_{f2m} and some pore structure parameters and petrophysical properties of carbonate core samples ((a) D_{f2m} and air permeability K_{air}; (b) D_{f2m} and displacement pressure p_d; (c) D_{f2m} and r_{50}; (d) D_{f2m} and r_{35}; (e) D_{f2m} and sorting coefficient S_p; (f) D_{f2m} and tortuosity τ).

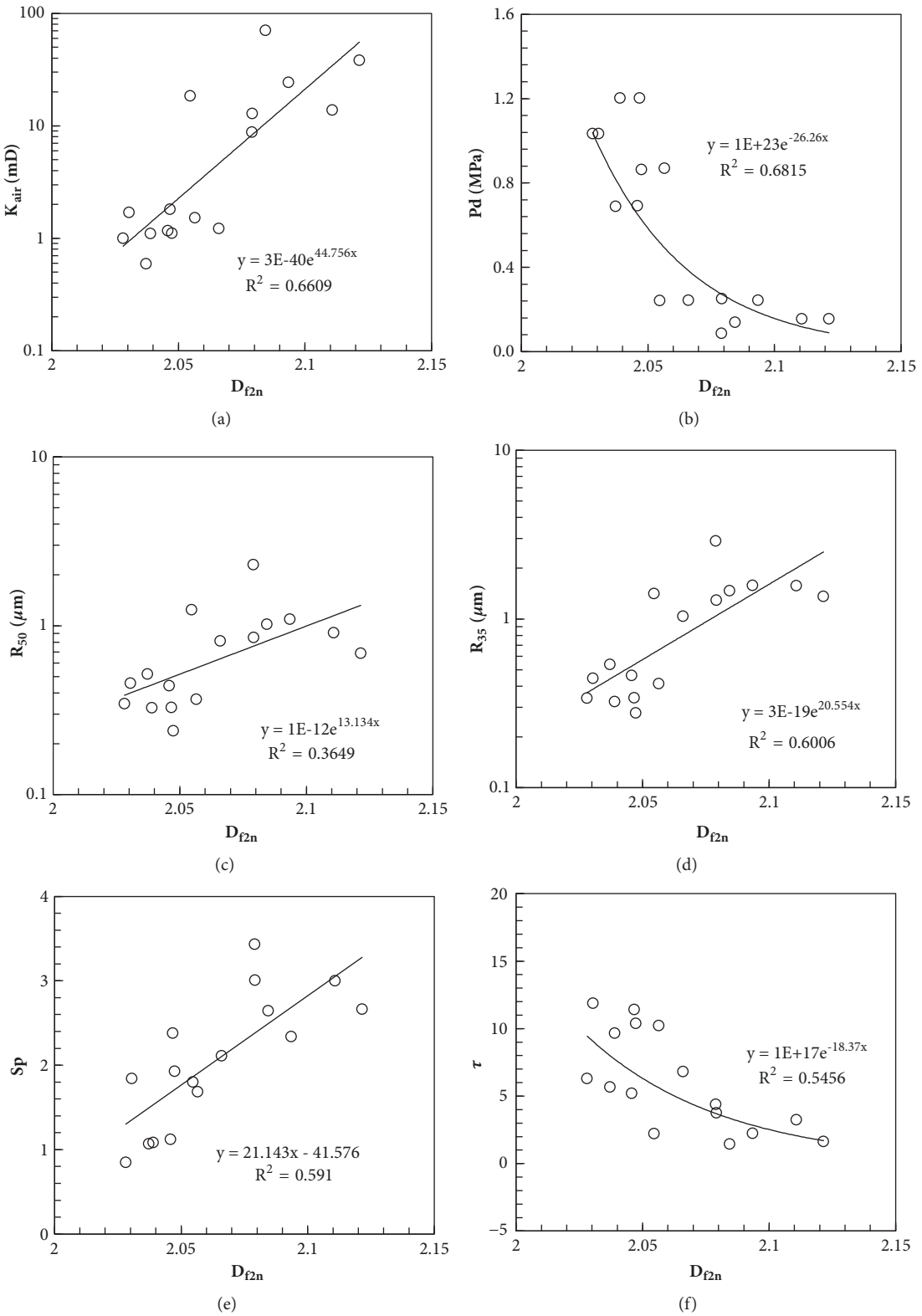

FIGURE 11: Relationship between fractal dimensions of nanoscale pores D_{f2n} and some pore structure parameters and petrophysical properties of carbonate core samples ((a) D_{f2n} and air permeability K_{air}; (b) D_{f2n} and displacement pressure p_d; (c) D_{f2n} and r_{50}; (d) D_{f2n} and r_{35}; (e) D_{f2n} and sorting coefficient S_p; (f) D_{f2n} and tortuosity τ).

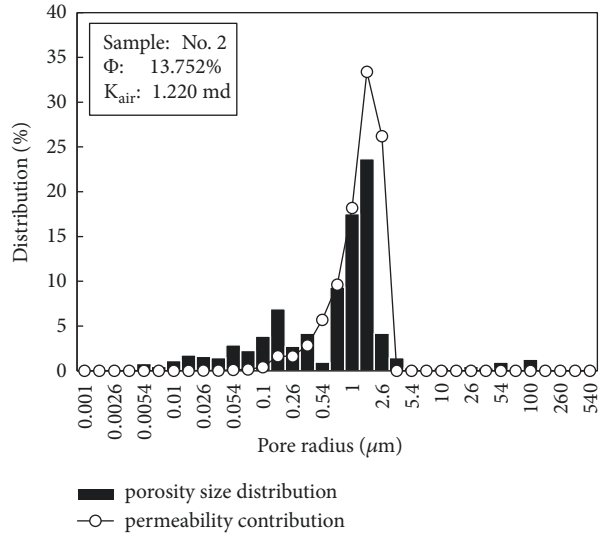

Figure 12: The distribution of pore volume and permeability contribution of the no. 2 core sample.

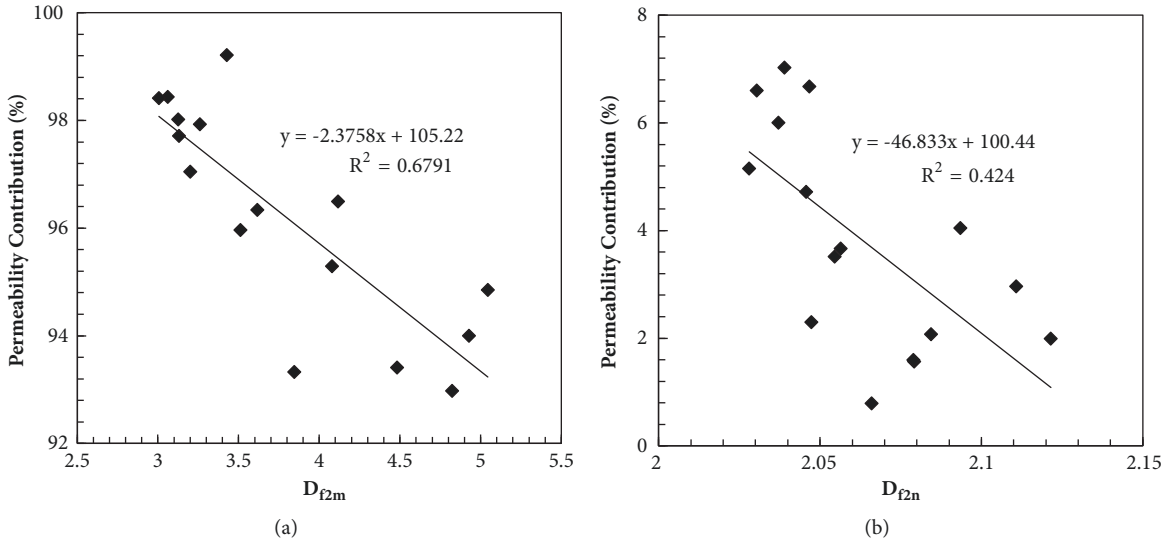

Figure 13: Relationship between fractal dimension and permeability contribution ((a) microscale pores; (b) nanoscale pores).

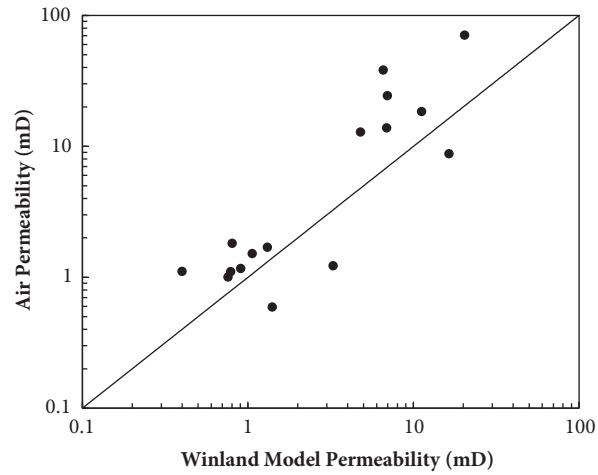

Figure 14: Comparison between the measured air permeability and the calculated permeability using Winland permeability model.

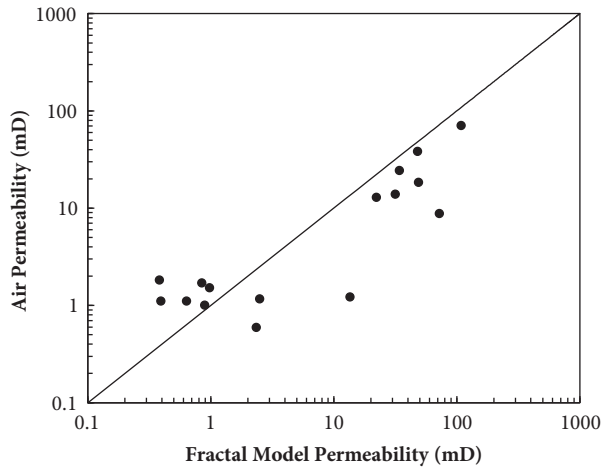

Figure 15: Comparison between the measured air permeability and the calculated permeability using fractal permeability model.

Table 5: The total pore volume and permeability contribution of microscale pores and nanoscale pores.

Core No.	Microscale pores		Nanoscale pores	
	Total pore volume S_{Hgm} (%)	Total permeability contribution K_{cm} (%)	Total pore volume S_{Hgn} (%)	Total permeability contribution K_{cn} (%)
1	50.00	97.93	44.69	2.07
2	55.00	99.21	39.52	0.79
3	55.81	96.34	36.55	3.66
4	60.83	95.29	35.40	4.71
5	64.73	93.41	28.16	6.60
6	64.34	94.00	33.01	6.00
7	68.93	94.85	28.65	5.15
8	54.04	93.33	35.75	6.67
9	61.16	97.71	28.97	2.29
10	61.51	92.98	34.10	7.02
11	61.45	96.49	35.10	3.51
12	49.84	98.44	41.61	1.56
13	45.31	95.96	47.54	4.04
14	41.45	98.01	52.26	1.99
15	41.77	97.04	51.20	2.96
16	46.04	98.41	43.73	1.59
Min	41.45	92.98	28.16	0.79
Max	68.93	99.21	52.26	7.02
Average	55.14	96.21	38.52	3.79

porous carbonates without visible fractures and vugs, and compared with Winland permeability model, the calculation results are acceptable.

Conflicts of Interest

The authors declare that there are no conflicts of interest regarding the publication of this paper.

Acknowledgments

This work was supported by the National Natural Science Foundation of China (no. 51604285), Beijing Municipal Natural Science Foundation (no. 3164048), Scientific Research Foundation of China University of Petroleum, Beijing (no. 2462017BJB11 and no. 2462016YQ1101), and the National Science Foundation for Young Scientists of China (Grant no. 41702359).

References

[1] F. Wang, Y. Li, X. Tang, J. Chen, and W. Gao, "Petrophysical properties analysis of a carbonate reservoir with natural fractures and vugs using X-ray computed tomography," *Journal of Natural Gas Science and Engineering*, vol. 28, pp. 215–225, 2016.

[2] B. Li, X. Tan, F. Wang, P. Lian, W. Gao, and Y. Li, "Fracture and vug characterization and carbonate rock type automatic classification using X-ray CT images," *Journal of Petroleum Science and Engineering*, vol. 153, pp. 88–96, 2017.

[3] B. B. Mandelbrot, *The Fractal Geometry of Nature*, Henry Holt and Company, San Francisco, Calif, USA, 1982.

[4] T. Dutta and S. Tarafdar, "Fractal pore structure of sedimentary rocks: Simulation by ballistic deposition," *Journal of Geophysical Research: Solid Earth*, vol. 108, no. 2, pp. 1–6, 2003.

[5] S. Feranie, U. Fauzi, and S. Bijaksana, "3D fractal dimension and flow properties in the pore structure of geological rocks," *Fractals. Complex Geometry, Patterns, and Scaling in Nature and Society*, vol. 19, no. 3, pp. 291–297, 2011.

[6] C. E. Krohn, "Sandstone fractal and Euclidean pore volume distributions," *Journal of Geophysical Research: Atmospheres*, vol. 93, no. 4, pp. 3286–3296, 1988.

[7] A. J. Katz and A. H. Thompson, "Fractal sandstone pores: implications for conductivity and pore formation," *Physical Review Letters*, vol. 54, no. 12, pp. 1325–1328, 1985.

[8] R. Angulo, V. Alvarado, and H. Gonzalez, "Fractal Dimensions from Mercury Intrusion Capillary Tests," in *Proceedings of the SPE Latin America Petroleum Engineering Conference*, Caracas, Venezuela.

[9] K. Li, "Analytical derivation of Brooks-Corey type capillary pressure models using fractal geometry and evaluation of rock heterogeneity," *Journal of Petroleum Science and Engineering*, vol. 73, no. 1-2, pp. 20–26, 2010.

[10] J. Lai and G. Wang, "Fractal analysis of tight gas sandstones using high-pressure mercury intrusion techniques," *Journal of Natural Gas Science and Engineering*, vol. 24, pp. 185–196, 2015.

[11] P. Li, M. Zheng, H. Bi, S. Wu, and X. Wang, "Pore throat structure and fractal characteristics of tight oil sandstone: A case study in the Ordos Basin, China," *Journal of Petroleum Science and Engineering*, vol. 149, pp. 665–674, 2017.

[12] Y. Cai, D. Liu, Z. Pan, Y. Che, and Z. Liu, "Investigating the Effects of Seepage-Pores and Fractures on Coal Permeability by Fractal Analysis," *Transport in Porous Media*, vol. 111, no. 2, pp. 479–497, 2016.

[13] Y. Yao, D. Liu, D. Tang et al., "Fractal characterization of seepage-pores of coals from China: an investigation on permeability of coals," *Computers & Geosciences*, vol. 35, no. 6, pp. 1159–1166, 2009.

[14] Y. Li, G. Q. Lu, and V. Rudolph, "Compressibility and Fractal Dimension of Fine Coal Particles in Relation to Pore Structure Characterisation Using Mercury Porosimetry," *Particle & Particle Systems Characterization*, vol. 16, no. 1, pp. 25–31, 1999.

[15] X. Liu and B. Nie, "Fractal characteristics of coal samples utilizing image analysis and gas adsorption," *Fuel*, vol. 182, pp. 314–322, 2016.

[16] H. Bu, Y. Ju, J. Tan, G. Wang, and X. Li, "Fractal characteristics of pores in non-marine shales from the Huainan coalfield, eastern China," *Journal of Natural Gas Science and Engineering*, vol. 24, pp. 166–177, 2015.

[17] L. Liang, J. Xiong, and X. Liu, "An investigation of the fractal characteristics of the Upper Ordovician Wufeng Formation shale using nitrogen adsorption analysis," *Journal of Natural Gas Science and Engineering*, vol. 27, pp. 402–409, 2015.

[18] C. E. Krohn, "Fractal measurements of sandstones, shales, and carbonates," *Journal of Geophysical Research: Atmospheres*, vol. 93, no. 4, pp. 3297–3305, 1988.

[19] S. Xie, Q. Cheng, Q. Ling, B. Li, Z. Bao, and P. Fan, "Fractal and multifractal analysis of carbonate pore-scale digital images of petroleum reservoirs," *Marine and Petroleum Geology*, vol. 27, no. 2, pp. 476–485, 2010.

[20] W. R. Purcell, "Capillary pressurestheir measurement using mercury and the calculation of permeability therefrom. Pet Trans AIME," *Journal of Petroleum Technology*, vol. 1, no. 2, pp. 39–48, 1949.

[21] S. Kolodzie, "Analysis of Pore Throat Size and Use of the Waxman-Smits Equation to Determine OOIP in Spindle Field Colorado," in *Proceedings of the SPE Annual Technical Conference and Exhibition*, Society of Petroleum Engineers, 1980.

[22] B. F. Swanson, "A Simple Correlation Between Permeabilities and Mercury Capillary Pressures," *Journal of Petroleum Technology*, vol. 33, no. 12, pp. 2498–2504, 1981.

[23] B. M. Yu and P. Cheng, "A fractal permeability model for bi-dispersed porous media," *International Journal of Heat and Mass Transfer*, vol. 45, no. 14, pp. 2983–2993, 2002.

[24] J. Cai, L. Luo, R. Ye, X. Zeng, and X. Hu, "Recent advances on fractal modeling of permeability for fibrous porous media," *Fractals*, vol. 23, no. 1, Article ID 1540006, 2015.

[25] J. J. M. Buiting and E. A. Clerke, "Permeability from porosimetry measurements: Derivation for a tortuous and fractal tubular bundle," *Journal of Petroleum Science and Engineering*, vol. 108, pp. 267–278, 2013.

[26] H. A. Nooruddin, M. E. Hossain, H. Al-Yousef, and T. Okasha, "Comparison of permeability models using mercury injection capillary pressure data on carbonate rock samples," *Journal of Petroleum Science and Engineering*, vol. 121, pp. 9–22, 2014.

[27] A. Mirzaei-Paiaman, H. Saboorian-Jooybari, and P. Pourafshary, "Improved Method to Identify Hydraulic Flow Units for Reservoir Characterization," *Energy Technology*, vol. 3, no. 7, pp. 726–733, 2015.

[28] E. W. Washburn, "The dynamics of capillary flow," *Physical Review A: Atomic, Molecular and Optical Physics*, vol. 17, no. 3, pp. 273–283, 1921.

[29] W. Friesen and R. Mikula, "Fractal dimensions of coal particles," *Journal of Colloid and Interface Science*, vol. 120, no. 1, pp. 263–271, 1987.

[30] B. Zhang and S. Li, "Determination of the Surface Fractal Dimension for Porous Media by Mercury Porosimetry," *Industrial & Engineering Chemistry Research*, vol. 34, no. 4, pp. 1383–1386, 1995.

[31] B. Zhang, W. Liu, and X. Liu, "Scale-dependent nature of the surface fractal dimension for bi- and multi-disperse porous solids by mercury porosimetry," *Applied Surface Science*, vol. 253, no. 3, pp. 1349–1355, 2006.

[32] Y. Cai, D. Liu, Y. Yao, J. Li, and J. Liu, "Fractal characteristics of coal pores based on classic geometry and thermodynamics models," *Acta Geologica Sinica*, vol. 85, no. 5, pp. 1150–1162, 2011.

[33] J.-L. Liu, C.-A. Tian, Y.-W. Zeng, and B. Dong, "Fractal dimensionality dependence of microstructural parameters and permeability in fractal porous media," *Shuikexue Jinzhan/Advances in Water Science*, vol. 17, no. 6, pp. 812–817, 2006.